Journal of Materials Science: Materials in Electronics (2019) 30:6564–6574
https://doi.org/10.1007/s10854-019-00963-4

Exploration of thermoacoustics behavior of water based nickel ferrite nanofluids by ultrasonic velocity method

Prashant B. Kharat[1] · S. D. More[2] · Sandeep B. Somvanshi[1] · K. M. Jadhav[1]

Received: 9 January 2019 / Accepted: 16 February 2019 / Published online: 25 February 2019

Abstract
Magnetic nanofluids (commonly known as ferrofluids) have captured the great attention of the researchers due to their various kinds of applications such as heat transfer, hyperthermia treatments, targeted drug delivery etc. The present experimental investigations deal with the thermoacoustic behaviour of the water based nanofluids of nickel ferrites. The magnetic nickel ferrite nanoparticles were produced by the simple and inexpensive chemical co-precipitation route. The prepared nanoparticles were exposed to different characterization tools for structural, morphological, compositional and magnetic properties analysis. X-ray diffraction analysis with Rietveld refinement confirmed the single phasic nature with nanometric crystallite size of the prepared nanoparticles. Scanning electron microscope images revealed the spherical and nanocrystalline morphology of the prepared nanoparticles. The M-H plot recorded at room temperature revealed the superparamagnetic nature of the nanoparticles. Further, the co-precipitated nickel ferrite nanoparticles with different concentrations were utilized for the preparation of the water based magnetic nanofluids. Colloidal stability of the prepared nanofluids was analyzed by UV–Vis spectroscopy technique and it revealed the stability over 11 days without separation in phase. The temperature dependent thermoacoustic properties of the prepared nanofluids were analyzed through Ultrasonic Interferometer. The interaction between particle–particle and particle–fluid are explained on the basis of thermo-acoustic parameters.

1 Introduction

Magnetic nanofluids (well known as ferrofluids) are nothing but a colloidal suspension of the nanosized magnetic nanoparticles sized in between 1 nm and 50 nm in the fluidic media. The magnetic nanofluids were demonstrated the blend of the duel properties i.e. the magnetic and additionally the fluidic [1]. The properties of the magnetic nanofluids like thermal conductivity, density, viscosity, acoustic etc can be easily tuned by introducing the guest magnetic field [2]. Pertaining to the novel properties at the nanoscale, nanoparticles have been broadly utilized in an assortment of uses, for example, medication, electronics, optics, manufacturing, catalysts, advance photovoltaics etc [3–7]. The customary liquids, for example, water, oil, ethylene glycol (EG), and so on were broadly utilized for the preparation of the nanofluids [8–10]. The ordinary liquids have low thermal properties with a correlation of the metals. The utilization of metal nanoparticles with little sum in an ordinary liquid improves these properties of the nanofluids [11, 12]. The ferromagnetic materials (for example, Fe, Co, Ni, Fe_3O_4 and other metal oxides) are generally utilized for this purpose and it demonstrated their impact on the properties of magnetic nanofluids [13]. The cubic spinel ferrites (MFe_2O_4, M is the divalent metal ion) are a vital class of the magnetic material which possess high saturation magnetization and great thermal properties [14, 15]. The magnetic interface and London-van der Waals forces are the fundamental driver's to settle down magnetic nanoparticles in the fluidic medium [16]. This agglomeration in the magnetic nanofluids can be overcome by a few strategies, for example, incorporation of a surfactants [17], ultrasonication [18], modifying pH esteem [19] of the nanofluids, and so forth.

The ultrasonic technique has turned into a useful asset for assessment of physicochemical properties of the materials. They have captured huge applications in fundamental science,

✉ Prashant B. Kharat
pbk9403750321@gmail.com

✉ K. M. Jadhav
drjadhavkm@gmail.com

[1] Department of Physics, Dr. Babasaheb Ambedkar Marathwada University, Aurangabad, Maharashtra 431001, India

[2] Department of Physics, Deogiri College, Aurangabad, Maharashtra 431001, India

industries and biochemical innovation [20]. Estimation of ultrasonic velocity and other determined parameters in dissolvable assumes basically an essential job in the investigation of the physicochemical conduct of solutions [21]. It figures some essential thermodynamic properties which give subjective data with respect to sub-atomic interactions [22].

In this respects, Leena et al. were readied TiO_2 NPs produced by sol–gel technique and prepared TiO_2–water nanofluid. The TiO_2 nanofluid at different volume divisions was characterized and particle size impact on the thermal properties of the nanofluids was examined in order to use it as a modern coolant. Likewise, acoustical parameters of TiO_2–water nanofluid were estimated and explored its impact on thermal properties of the nanofluids [23]. M. Leena et al. in another report, blended unadulterated zinc oxide (ZnO), cerium (Ce) doped ZnO, lanthanum (La) doped ZnO and cerium-lanthanum (Ce-La) doped ZnO nanoparticles (NPs) by the wet chemical technique. Further, they prepared the nanofluids by dispersing it into the water and blended comprehensively by the method for ultrasonication process. Likewise, they also evaluated thermal conductivity of ZnO-water nanofluid by ultrasonic velocity estimations system [21]. P. B. Kharat et al. prepared superparamagnetic cobalt ferrite nanoparticles and utilized it to prepare ferrofluids by dispersing them into ethylene glycol (EG). Likewise in this report, they explained the detailed thermoacoustic examination of the cobalt ferrite–EG nanofluids [24]. Anu K. et al. synthesized water-based magnetite nanofluids of different Zn-doping through co-precipitation route. Acoustical parameters, for example, adiabatic compressibility, mean free path, acoustic impedance, Rao's constant and Wada's constant are inferred and investigated in this work [25]. M. Nabeel Rashin et al. examined ultrasonic conduct of cobalt ferrite nanofluids of different concentrations prepared through co-precipitation strategy [26].

In this light, we have performed the thermoacoustic investigation of nickel ferrite – water nanofluids by ultrasonic velocity technique. The nanoparticles of the nickel ferrite were fabricated by the chemical coprecipitation method. The structural, morphological, compositional and magnetic analysis of the prepared nanoparticles was described. Further, the thermoacoustic properties, such as, Ultrasonic Velocity (U), Acoustic Impedance (Z), Adiabatic Compressibility (β), Bulk Modulus (K), Ultrasonic Attenuation (α), Relaxation Time (τ), and Intermolecular Free Length (Lf) were assessed and inspected in the present work.

2 Materials and methods

2.1 Materials

The AR grade raw materials such as Nickel (II) nitrate hexahydrate (Ni $(NO_3)_2{\cdot}6H_2O$), Ferric (III) nitrate nonahydrate (Fe $(NO_3)_3{\cdot}9H_2O$)), Sodium hydroxide (NaOH), Acetone (CH_3COCH_3), DI water (H_2O) and Nitric acid 69% (HNO_3), were purchased from Merck Millipore and used for the synthesis of nickel ferrite nanoparticles as received without any purification process.

2.2 Synthesis of nickel ferrite nanoparticles and preparation of nanofluids

For the synthesis of the nickel ferrite magnetic nanoparticles, the nitrates of nickel and ferric are independently stirred to get a precusor solution in 1:2 stoichiometric proportion. Both the solutions were combined and stirred for 1.5 h to get a homogeneous mixture. The pH estimation of the homogeneous mixture was estimated and it was observed to be 3. The 2 M NaOH pellets were dissolved in water independently and used to maintain the pH of the prepared solution. The drop by drop NaOH solution was included the precusor solution and accomplished the pH at 9. The pH maintained precusor solution was uniformly heated at 90 °C for the 2 h until the darker precipitation of the nickel ferrite was acquired. The prepared dark colored precipitation was then washed several times with DI water and 2 M HNO_3 solution for evacuate impurities presented in the prepared nickel ferrite precipitate. Additionally, the precipitate was also washed by utilizing the DI water and ethanol. The washed precipitate was uniformly dried in a microwave heater over the night at the 60 °C. The magnetic nanofluids of nickel ferrite nanoparticles were prepared by utilizing two-step method by dispersing the acquired nickel ferrite nanoparticles in the water in different convergences of (0.2%, 0.4%, 0.6%, 0.8%, and 1% by volume). The prepared nickel ferrite—water magnetic nanofluids were ultrasonicated for 3 h to decrease the magnetic interaction agglomeration of the nanoparticles in the water as per the expounded flowchart and procedure of preparation of the nanofluids given in our past reports [16].

3 Characterizations

3.1 Properties of $NiFe_2O_4$ nanoparticles

The structural, morphological, compositional and magnetic investigation of prepared nickel ferrite nanoparticles was contemplated by utilizing X-ray beam diffractometer (XRD), Field Emission Scanning Electron Microscope (FE-SEM), Energy Dispersive X-Ray Spectroscopy (EDS), and Vibrating Sample Magnetometer (VSM). X-ray diffractometer (BRUKER D8 Advance) with Cu-Kα radiation ($\lambda = 1.5418$ Å) in the 2θ range from 20° to 80° were utilized for phase formation and spinel cubic structure investigation of the $NiFe_2O_4$ magnetic nanoparticles. The

room temperature XRD pattern was compared with Joint Committee on Powder Diffraction Standards (JCPDS) (card number-10-0325). Using FE-SEM images, the grain size and morphology of the prepared nanoparticles were determined. The room temperature magnetic behaviour of the prepared nanoparticles was studied using VSM. Using VSM data, the values of saturation magnetization, coercivity and remenance magnetization were determined. The colloidal steadiness of nanofluids was examined by the UV–Vis spectroscopy technique.

3.2 Thermo-acoustic properties of nanofluids

The thermo-acoustic properties of $NiFe_2O_4$—water nanofluids were studied by utilizing the Ultrasonic Interferometer. The ultrasonic interferometer is a basic and straight forward technique which yields precise and steady information, from which one can decide the velocity of ultrasonic sound in a fluid medium and magnetic nanofluids with a high level of exactness (±0.01%). A crystal controlled interferometer (Model F-05) provided by Mittal Enterprises, New Delhi, with 2×10^6 Hz operating frequency was utilized to quantify the ultrasonic velocity [27]. A twofold walled round and hollow estimating cell was utilized to keep up a steady temperature of the nanofluids specimen during the total measurements. The estimations of the ultrasonic velocity (v) depended on precise investigation of the wavelength (λ) in the nanofluids specimen. For the investigations, the ultrasonic waves of 2×10^6 Hz were delivered by a quartz plate which is put at the base of the estimating cell. The Ultrasonic waves were replicated by a compact metal dish held in similar to the quartz dish. In the event, the separation between these dishes is decisively kept to capture a whole range of the sound wavelength. The ultrasonic waves were delivered from the quartz plate which makes acoustic reverberation in the nanofluids specimen and gives an electrical yield which gives most noteworthy anode current of the generator. While expanding or diminishing the separation precisely to one-half wavelength (λ/2) or multiple in that, makes the anode current to its most astounding worth.

From the information of wavelength (λ) the velocity (v) and frequency (f) can be gained by the Eq. (1):

$$V = \lambda \times f \tag{1}$$

The estimations of the viscosity, density, specific heat etc values by assessing thermo-acoustical properties is reported in our past report [28]. Thermo-acoustical properties viz. Ultrasonic Velocity (U), Acoustic Impedance (Z), Adiabatic Compressibility (β), Bulk Modulus (K), Ultrasonic Attenuation (α), Relaxation Time (τ) and Intermolecular Free Length (Lf) were evaluated and analyzed in the present work. The steady temperature bath was utilized to settle the temperature of the specimens. The ultrasonic estimations were carried twice and the normal estimations of the average estimation were recorded for all the thermo-acoustical estimations.

4 Results and discussion

4.1 Structural, morphological, elemental and magnetic analysis

The structural examination of the nickel ferrite nanoparticles was investigated by the X-ray beam diffraction. The observed X-Ray diffractogram confirmed that the prepared nanoparticles possess the Fd3mO_7^h space group and well nano crystallinity. The X-Ray diffractogram gives clear proof of the Bragg's reflection peaks well matching to the cubic spinel ferrites [29]. In order to detailed structural study the Rietveld refinement of the XRD data was carried out with the help of FullProf software and refined x-ray pattern is shown in Fig. 1. The Rietveld [30] refined structural parameters are recorded in Table 1.

The FE-SEM micrographs of $NiFe_2O_4$ were appeared in Fig. 2a, b. The FE-SEM micrographs demonstrate that the nickel ferrite nanoparticles possess spherical morphology and homogeneous distribution of the grains. The nanometric range of average grain size confirmed nano crystallinity of the prepared nanoparticle. It seems to be grains are agglomerated to the some extent which ascribed to the high surface vitality and magnetic interface between the prepared nanoparticles [31]. Along these lines, a portion of the lengthened particles are also seen in FE-SEM micrographs.

The compositional spectrum of the prepared nanoparticles is appeared in Fig. 3. The compositional spectrum demonstrates the peaks belonging to the present components in nickel ferrite nanoparticle. The percentage is appeared in

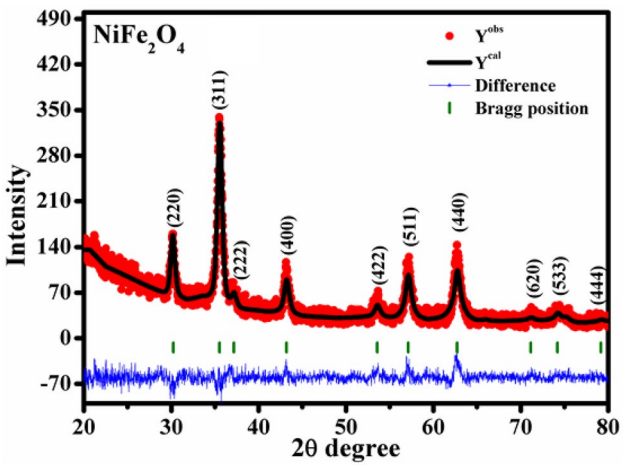

Fig. 1 X-ray diffraction pattern of the nickel ferrite nanoparticles

Table 1 Molecular weight (M_w), Lattice constant (a), crystallite size (D), particle size (D′), Specific Surface Area (SSA), X-ray density (ρ_{XRD}), Bulk density (ρ_{BULK}), Porosity (Pt) of oleic acid coated nickel ferrite nanoparticles

Sample	M_w (g/mol)	a (Å)	D (nm)	D′ (nm)	SSA (m^2/g)	ρ_{XRD} (g/cm^3)	ρ_{BULK} (g/cm^3)	Pt (%)
$NiFe_2O_4$	234.38	8.355	10.40	9.5 ± 2	115.94	5.336	3.633	31.83

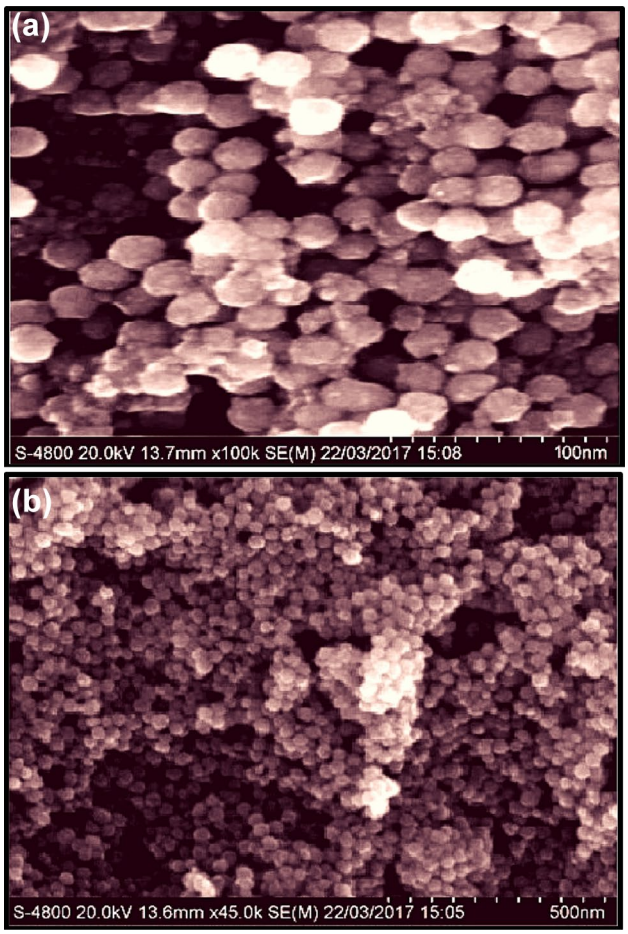

Fig. 2 **a**–**b** FE-SEM micrograph of the nickel ferrite nanoparticles

the inset of the Fig. 3. The compositional spectrum also reveals the absence of impurities uncovering the purity of the prepared sample. The acquired atomic proportion of Ni, Fe, and O coordinate well with that of expected and keeps up the stoichiometric extent. The small additional peaks also observed which may be attributed to the Carbon, which is not detected correctly by EDS analysis that is due to the substrate used while sample preparation for the EDS analysis.

The room temperature recorded M-H curve of the prepared nanoparticles is shown in Fig. 4. From the M-H curve, the magnetic parameters i.e. saturation magnetization (M_S), coercivity (H_C) and remanent magnetization (M_r) are estimated and are listed in Table 2. The prepared nanoparticles possess high saturation magnetization (M_S) and modest remanent magnetization (M_r) with avoidable coercivity (H_C) value, which demonstrates that the prepared nanoparticle appears superparamagnetic nature [32].

4.2 Colloidal stability analysis

The colloidal stability of the prepared $NiFe_2O_4$–water nanofluid specimen was evaluated from UV–Vis spectroscopy. Figure 5 demonstrates UV–Vis absorption spectrum for $NiFe_2O_4$–water nanofluid for 1.0% volume fraction. The observed UV–Vis absorption spectrum gives the idea that the most extreme absorption was seen at wavelength of $\lambda = 272$ nm. Figure 6 shows the Plot of absorbance versus time recorded at 272 nm for $NiFe_2O_4$–water nanofluid (1.0%). The specimen was scrutinized for 12 days and maximum absorption was stayed steady till seventh day for the 1.0% volume fraction. This uncovers the present nanofluids specimen of 1.0% volume portion was steady for seven days as seen from Fig. 6.

Similar to this, the UV–Vis absorption range was investigated for the whole Vol. % i.e. (0.2%, 0.4%, 0.6%, 0.8%, and 1%) which is set up in the present investigation. The most astounding steadiness saw from the absorption range of over 11 days without phase separation was observed for the 0.2% volume portion. The colloidal stability of the considerable number of specimens is recorded in the Table 3.

4.3 Thermoacoustic analysis

The thermoacoustic examination enables us to decide different parameters through which various thermophysical properties of the nanofluids can be an adventurer. The acoustic examination can be giving a potential and conservative option in contrast to the exact assurance of the thermal conductivity of magnetic nanofluids, which has been an impressive test, utilizing the accessible instruments.

4.3.1 Ultrasonic velocity (U)

The temperature relied upon variety in ultrasonic velocity is plotted and appeared in Fig. 7. It is observed that, the ultrasonic velocity of the prepared nanofluid diminishes with the expansion of nanoparticle content.

The ultrasonic velocity at 20 °C is diminished with expanding volume portion from 1482 m/s (for 0.0 vol%), (−0.47%) 1475 m/s (for 0.2 vol%), (−0.82%) 1463 m/s (for 0.6 vol%)

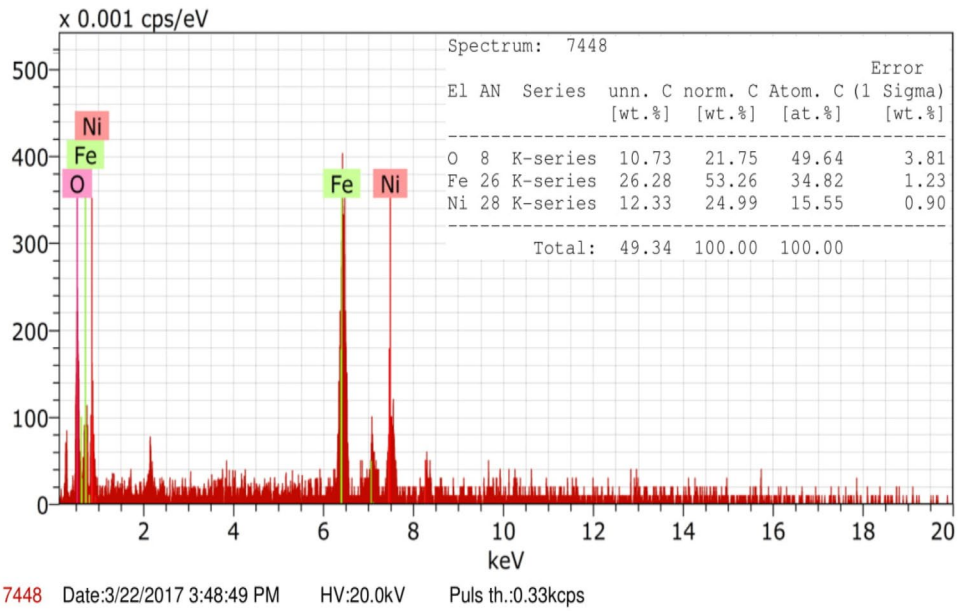

Fig. 3 EDS spectrum of the nickel ferrite nanoparticles

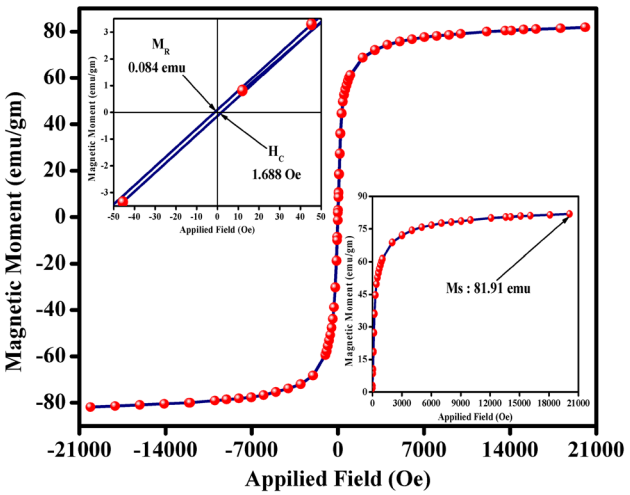

Fig. 4 M-H hysteresis curve of the nickel ferrite nanoparticles

and (−0.90%) 1450 m/s (for 1.0 vol%) and comparable pattern was observed for all the temperature ranges. Further, the ultrasonic velocity diminished at 80 °C i.e. 1527 m/s (for 0.0 vol%), 1522 m/s (for 0.2 vol%), 1511 m/s (for 0.6 vol%) and 1501 m/s (for 1.0 vol%). This decline in ultrasonic velocity with an expansion in nanoparticle concentration is perceived by the $NiFe_2O_4$–water interface, and it further affirms the strength of intermolecular associations over the intramolecular interactions [33]. Also, with the molecule stacking, there is a probability for diminishing the rate of event of Brownian movement of the liquid atom, alongside the arrangement for the resistive surface layer that can induce a decline in ultrasonic velocity [34]. Moreover, with an expansion in nanoparticle conc. there is an increment in density which likewise adds to the decrease in velocity. At the higher temperature range, the rate of decrement in velocity concerning conc. somewhat decreases in magnitude [35]. Thus, it demonstrates the most of the $NiFe_2O_4$–water interface over particle–particle collaboration at higher temperatures too.

Figure 7 additionally uncovers the progressions in ultrasonic velocity concerning the temperature. From the observed outcomes, it is cleared that the ultrasonic velocity in the $NiFe_2O_4$-water nanofluids increments with expanding the temperature. The ultrasonic velocity for unadulterated water i.e. 0.0 vol% were expanded from 1482 m/s (20 °C), (+3.04%) 1527 m/s (40 °C), (+1.64%) 1552 m/s (60 °C) and (+0.19%) 1527 m/s (80 °C). For 0.2 Vol. % it expanded from 1475 m/s (20 °C), (+3.12%) 1521 m/s (40 °C), (+1.58%) 1545 m/s (60 °C) and (+0.26%) 1549 m/s (80 °C) and comparable pattern were observed for the different temperatures. At long last, for 1.0 Vol. % was expanded 1450 m/s (20 °C), (+3.17%) 1496 m/s (40 °C), (+1.60%) 1520 m/s (60 °C) and (+0.20%) 1523 m/s (80 °C).

Table 2 Saturation magnetization (M_S), Remanence magnetization (M_R), Coercivity (H_C), the effective anisotropy constant (K_{eff}), surface anisotropy (K_S), magnetic moment per formula unit (η_H), maximum magnetic diameter (D_M) of $NiFe_2O_4$ nanoparticles

Sample	M_S (emu/g)	M_R (emu)	H_C (Oe)	K_{eff} (10^5 erg/cm^3)	K_S (10^{-2} erg/cm^2)	η_H (μ_B)	D_M (nm)
$NiFe_2O_4$	81.912	0.084	1.688	1.14	0.78	3.21	8.76

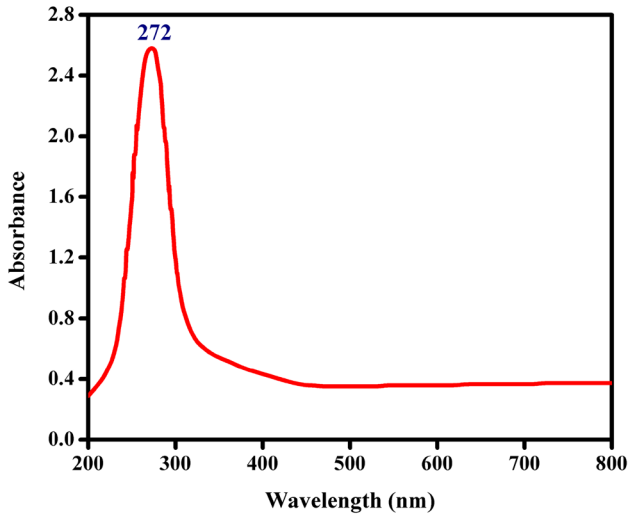

Fig. 5 UV–Vis absorption spectrum for $NiFe_2O_4$–water nanofluid (1.0%)

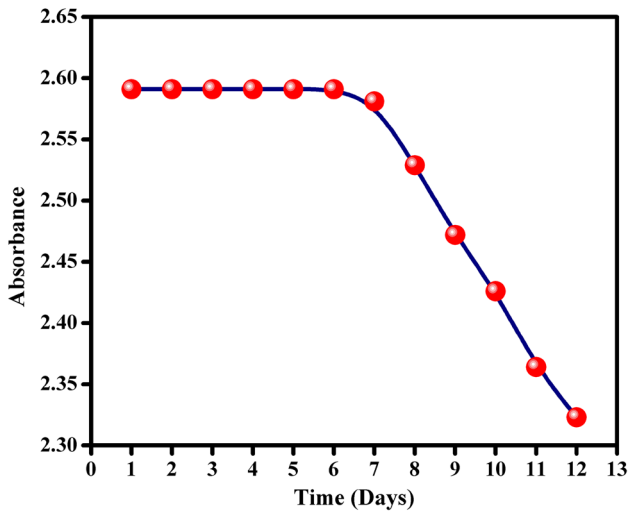

Fig. 6 Plot of absorbance versus time recorded at 272 nm for $NiFe_2O_4$–water nanofluid (1.0%)

Table 3 Colloidal Stability for oleic acid functionalized $NiFe_2O_4$–water nanofluid

Concentration (vol. %)	Colloidal stability (days)
0.2	12
0.4	11
0.6	9
0.8	9
1.0	7

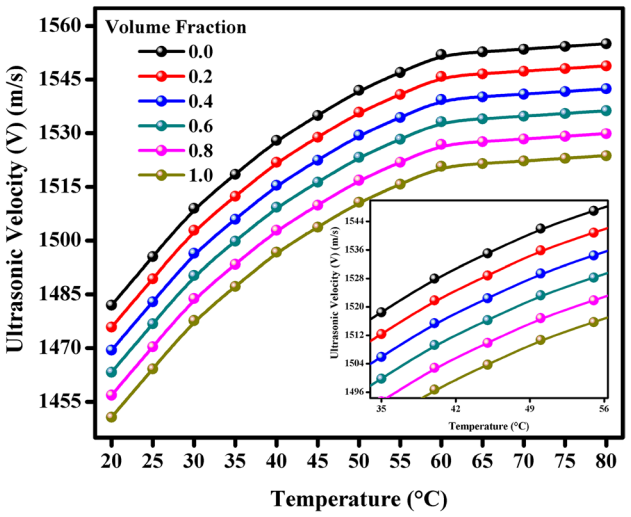

Fig. 7 Temperature-dependent ultrasonic velocity of NiFe2O4 - water nanofluids

It appears that the magnetic nanofluids pursue the outstanding conduct of water demonstrating an expansion in velocity with an increment in temperature that can be clarified utilizing the open and close-packed structure of water molecule. Water comprises of hydrogen-reinforced groups and unbounded water atoms. The particles in the inside groups are quadrupled fortified and unbounded water atoms should involve the space between the clusters [36]. These clusters are now and then alluded to as open structured water and the dense monomeric liquid is alluded to as closed structured water. In water, the ascent in temperature causes warm break of the open packed structure of water, which thus, improves the attachment of water atoms and less compressible closed structure prompting an expansion in the ultrasonic velocity [37].

4.3.2 Acoustic impedance (Z)

The acoustic impedance of the nanofluids as for different nanoparticles conc. is appeared in Fig. 8. The acoustic impedance of nanofluid was assessed by the Eq. (2),

$$Z = \rho \times U \tag{2}$$

where the Z is the acoustic impedance, ρ is the thickness and U is the ultrasonic velocity of the nanofluids.

From the observed outcomes, it tends to be seen that the acoustic impedance of the nanofluids was expanded with expanding the nanoparticles conc. In the case of 20 °C the acoustic impedance were expanded with expanding volume part from 1478×10^3 Ns/m^3 (for 0.0 vol%), (0.74%) 1489×10^3 Ns/m^3 (for 0.2 vol%), 1.21% 1507×10^3 Ns/m^3 (for 0.6 vol%) and 1.19%) 1525×10^3 Ns/m^3 (for 1.0 vol%) and comparative pattern observed for all the temperature.

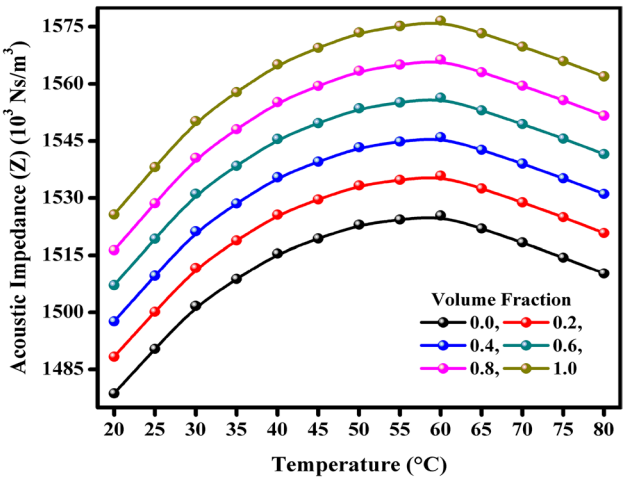

Fig. 8 Temperature-dependent acoustic impedance of $NiFe_2O_4$–water nanofluids

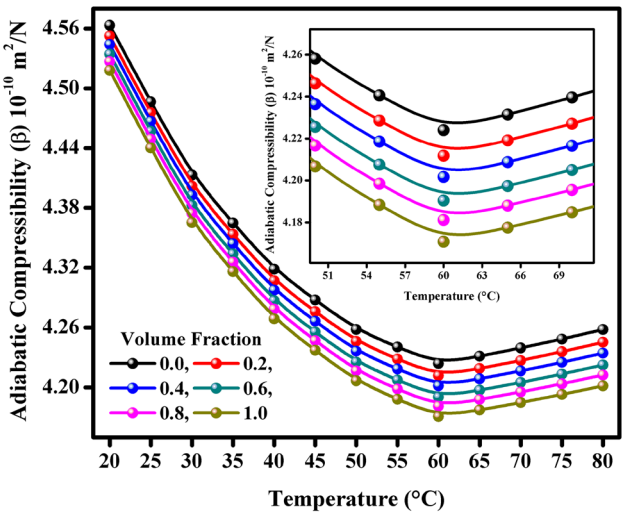

Fig. 9 Temperature-dependent adiabatic compressibility of $NiFe_2O_4$–water nanofluids

Moreover, the acoustic impedance increments at 80 °C with expanding volume part from 1510×10^3 Ns/m^3 (for 0.0 vol%), (0.73%) 1521×10^3 Ns/m^3 (for 0.2 vol%), (1.25%) 1540×10^3 Ns/m^3 (for 0.6 vol%) and (1.43%) 1562×10^3 Ns/m^3 (for 1.0 vol%).

4.3.3 Adiabatic compressibility (β)

The adiabatic compressibility of the nanofluids concerning different nanoparticles conc. is appeared in Fig. 9. Equation (3) was utilized for the assessment of adiabatic compressibility of the nanofluids,

$$\beta = \frac{1}{U^2 \times \rho} \tag{3}$$

where β is the adiabatic compressibility, U is the ultrasonic speed and ρ is the thickness of the nanofluids.

The observed outcomes demonstrate that, the adiabatic compressibility of the nanofluids was diminished with expanding the nanoparticles conc. Further, the adiabatic compressibility increments in the range of 60 °C to 80 °C with expanding temperature and diminishing with expanding nanoparticles volume portion. In the case of 20 °C the adiabatic compressibility were diminishes with expanding nanoparticles volume division from 4.562×10^{-10} m^2/N (for 0.0 vol%), (−0.20%) 4.553×10^{-10} m^2/N (for 0.2 vol%), (−0.38%) 4.535 m/s (for 0.6 vol%) and (−0.40%) 4.517×10^{-10} m^2/N (for 1.0 vol%) and comparable pattern observed for all the temperature up to 60 °C. The decrease in the adiabatic compressibility with the expanding conc. uncovers that the particles might be firmly packed and less ionic repulsion exists between the water molecules. This additionally demonstrates the bond strength is improved at higher nanoparticle conc. [38], diminishing up to 60 °C, 4.225×10^{-10} m^2/N (for 0.0 vol%), (−2.176%) 4.217×10^{-10} m^2/N (for 0.2 vol%), (−2.089%) 4.190 m/s (for 0.6 vol%) and (−2.296%) 4.170×10^{-10} m^2/N (for 1.0 vol%).

Further, the adiabatic compressibility increments in the range of 60 °C to 80 °C with expanding temperature and diminishing with expanding nanoparticles volume portion from 80 °C, 4.258×10^{-10} m^2/N (for 0.0 vol%), (0.80%) 4.245×10^{-10} m^2/N (for 0.2 vol%), (0.663%) 4.222 m/s (for 0.6 vol%) and (0.74%) 4.201×10^{-10} m^2/N (for 1.0 vol%). This expansion in the adiabatic compressibility of the nanofluids may conceivable on the grounds that the rate of Brownian movement of the liquid particles was expanded and diminished in the density at 80 °C [39]. The varieties at different temperatures in the adiabatic compressibility of the nanofluids were additionally appeared in Fig. 9.

4.3.4 Bulk modulus (K)

The bulk modulus demonstrates the versatile properties of the nanofluids, which is a decided from the unbending nature of the nanofluid medium. The bulk modulus of the nanofluids is the complementary of the adiabatic compressibility of the nanofluids and evaluated by the Eq. (4),

$$K = U^2 \times \rho \tag{4}$$

where K is the mass modulus, U is the ultrasonic speed and ρ is the thickness of the nanofluids.

The bulk modulus of the nanofluids as for different nanoparticles conc. is appeared in Fig. 10. From the observed outcomes, it is revealed that the bulk modulus of the nanofluids was expanded with expanding the nanoparticles conc. and

further diminished with expanding temperature in the range of 60 °C to 80 °C.

4.3.5 Ultrasonic attenuation (α)

The ultrasonic attenuation is the damping of the acoustical vitality because of the absorption and the dissipating happens, which is likewise representing to the vitality loss of sound engendering in the nanofluids [40]. The ultrasonic attenuation was assessed by the Eq. (5),

$$\alpha = \frac{8\pi^2\eta}{3\rho U^3} \times f^2 \tag{5}$$

where α is the ultrasonic lessening, η is the consistency, ρ is the thickness and U is the ultrasonic speed of the nanofluids. The ultrasonic attenuation of the nanofluids as for different nanoparticles conc. is appeared in Fig. 11. From the observed outcomes, it very well may be seen that the ultrasonic attenuation of the nanofluids was expanded with expanding the nanoparticles conc.

4.3.6 Relaxation time (τ)

In violent stream, the prevailing slip instrument is resolved from accepting an inertial trip of the nanoparticle following a sudden stop of the eddy conveying the particle [41].

The relaxation time of the Brownian movement of nanoparticles in the nanofluids was assessed by the Eq. (6),

$$\tau = \frac{4\beta\eta}{3} \tag{6}$$

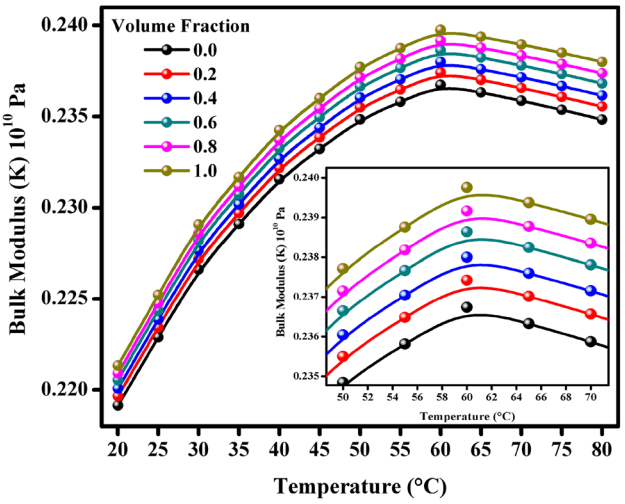

Fig. 10 Temperature-dependent bulk modulus of $NiFe_2O_4$/water nanofluids

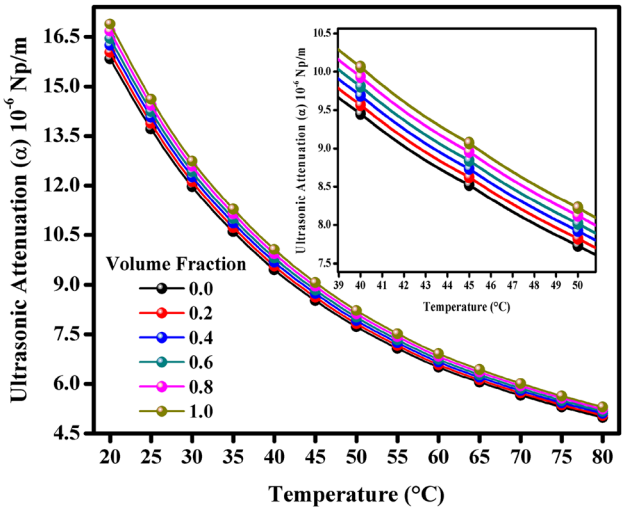

Fig. 11 Temperature-dependent ultrasonic attenuation of $NiFe_2O_4$/water nanofluids

where τ is the unwinding time, β is the adiabatic compressibility, and η is the viscosity of the nanofluids.

The relaxation time of the nanofluids concerning different nanoparticles conc. is appeared in Fig. 12. From the observed outcomes, it tends to be seen that the relaxation time of the nanofluids was expanded with expanding the nanoparticles concentration.

The long relaxation time of the Brownian movement of nanoparticles extensively influences to enhance the heat transporting properties of nanofluids [42]. The relaxation time (τ) can likewise been utilized to gauge the successful heat conductivity of nanofluids.

4.3.7 Intermolecular free length (L_f)

The intermolecular free length of the nanofluids regarding different nanoparticles conc. is appeared in Fig. 13. From the observed outcomes, it tends to be seen that the intermolecular free length of the nanofluids was diminished with expanding the nanoparticles conc. Moreover, Fig. 13 likewise demonstrates the impact of temperature on the $NiFe_2O_4$–water nanofluids and it is diminished with expanding temperature in the range of 20 °C to 40 °C. Forward with 40 °C it was again expanding with expanding temperature up to 80 °C.

The intermolecular free lengths were assessed by the Eq. (7),

$$L_f = \frac{K_T \times \beta}{2} \tag{7}$$

where L_f is the intermolecular free length, K_T is the Jacobson steady Temperature depended values are utilized are

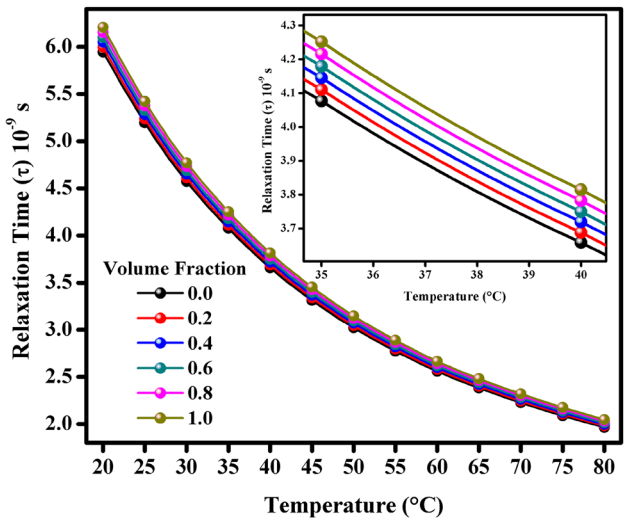

Fig. 12 Temperature-dependent relaxation time of $NiFe_2O_4$/water nanofluids

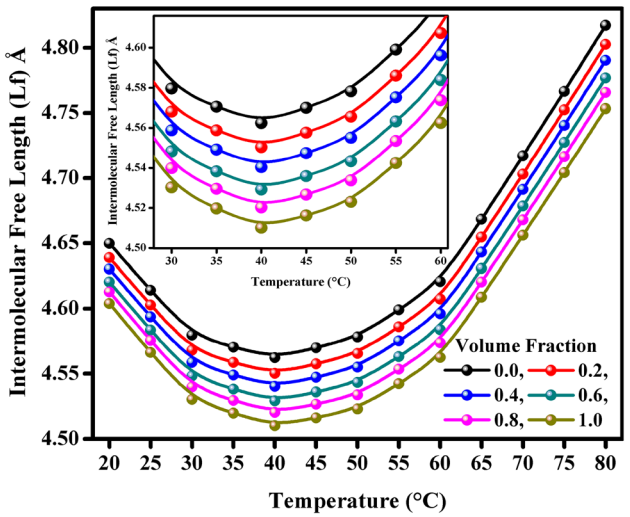

Fig. 13 Temperature-dependent intermolecular free length of NiFe2O4 / water nanofluids

given in the Table 4, and β is the adiabatic compressibility of the nanofluids.

In the comprehension of larger forces of interface between $NiFe_2O_4$ nanoparticles and water molecules shaping hydrogen holding, there will be a decline in free length in the water [43]. Free volume is clarified as the normal volume in which the focal particle can move inside the hypothetically determined cell uninhibitedly without accepting misrepresented by the aversion of the encompassing [37].

5 Conclusions

The present work demonstrated the thermoacoustic behaviour of the water based nanofluids of nickel ferrite nanoparticles. The nickel ferrite ($NiFe_2O_4$) nanoparticles were successfully synthesized by the chemical coprecipitation route. The major conclusions drawn from the results and discussion are as follows:

- Rietveld refined XRD patterns confirmed the monophasic and nanocrystalline behaviour of the prepared nickel ferrite nanoparticles.
- FE-SEM images revealed the spherical morphology and nanocrystallinity of the prepared nickel ferrite nanoparticles.
- Compositional spectrum confirmed the desired stoichiometric proportion with fine purity of the prepared nickel ferrite nanoparticles.
- Magnetic behaviour revealed the superparamagnetism in the prepared nickel ferrite nanoparticles.
- Colloidal stability of the prepared nickel ferrite–water nanofluids revealed the stability over 11 days without separation in phase.
- Thermoacoustic investigations gave the potential and inexpensive choice as contrasted with other ordinary techniques, for example, DLS, Particle estimate analyzer, thermal conductivity estimation systems etc to measure the exact thermophysical properties. It likewise illustrates particle–particle and fluid-particle interface of the prepared nanofluids.

Table 4 Jacobson constant (K_T) values over the temperature range 20 °C to 80 °C

Temperature °C	20	25	30	35	40	45	50	55	60	65	70	75
K_T = Jacobson constant	2.038	2.056	2.075	2.094	2.110	2.131	2.150	2.169	2.187	2.206	2.225	2.243

References

1. S. Angayarkanni, J. Philip, Review on thermal properties of nanofluids: recent developments. Adv. Colloid Interface Sci. **225**, (2015) 146–176
2. J.K. Patel, K. Parekh, Effect of carrier and particle concentration on ultrasound properties of magnetic nanofluids. Ultrasonics **55**, 26–32 (2015)
3. A.R. Chavan, R.R. Chiller, P.B. Kharat, K. Jadhav, Effect of Annealing temperature on structural, morphological, optical and magnetic properties of $NiFe_2O_4$ thin films. J. Supercond. Novel Magn. (2018). https://doi.org/10.1007/s10948-018-4565-3
4. J.S. Kounsalye, P.B. Kharat, A.R. Chavan, A.V. Humbe, R. Borade, K. Jadhav, Symmetry transition via tetravalent impurity and investigations on magnetic properties of Li0. 5Fe2. 5O4, in AIP Conference Proceedings, AIP Publishing, pp. 050067 (2018)
5. M.V. Shisode, A.V. Humbe, P.B. Kharat, K. Jadhav, Influence of Ba^{2+} on opto-electric properties of nanocrystalline $BiFeO_3$ multiferroic. J. Electron. Mater. https://doi.org/10.1007/s11664-018-6715-6 (2018)
6. S.B. Kale, B. Sandeep, M.N. Somvanshi, S.D. Sarnaik, S.J. More, Shukla, K.M. Jadhav, Enhancement in surface area and magnetization of CoFe2O4 nanoparticles for targeted drug delivery application. In: AIP Conference Proceedings, vol. 1953, no. 1, p. 030193. AIP Publishing (2018)
7. P.G. Undre, B. Prashant, R.V. Kharat, Kathare, K.M. Jadhav, Ferromagnetism in Cu2+ doped ZnO nanoparticles and their physical properties. J. Mater. Sci. https://doi.org/10.1007/s10854-019-00688-4 (2019)
8. P.B. Kharat, M. Shisode, S. Birajdar, D. Bhoyar, K. Jadhav, Synthesis and characterization of water-based $NiFe_2O_4$ ferrofluid. In: AIP Conference Proceedings, AIP Publishing, pp. 050122 (2017)
9. P.B. Kharat, S.B. Somvanshi, J.S. Kounsalye, S.S. Deshmukh, P.P. Khirade, K. Jadhav, Temperature-dependent viscosity of cobalt ferrite/ethylene glycol ferrofluids. In: AIP Conference Proceedings, AIP Publishing, pp. 050044 (2018)
10. B. Nigam, S. Mittal, A. Prakash, S. Satsangi, P. Mahto, B.P. Swain, Synthesis and Characterization of Fe3O4 Nanoparticles for Nanofluid Applications-A Review, in IOP Conference Series: Materials Science and Engineering, IOP Publishing, pp. 012187 (2018)
11. M. Shisode, P.B. Kharat, D.N. Bhoyar, V. Vinayak, M. Babrekar, K. Jadhav, Structural and multiferroic properties of Ba2 + doped BiFeO3 nanoparticles synthesized via sol-gel method. In: AIP Conference Proceedings, AIP Publishing, pp. 030276 (2018)
12. A. Yasinskiy, J. Navas, T. Aguilar, R. Alcántara, J.J. Gallardo, A. Sánchez-Coronilla, E.I. Martín, D. De Los Santos, C. Fernández-Lorenzo, Dramatically enhanced thermal properties for TiO2-based nanofluids for being used as heat transfer fluids in concentrating solar power plants. Renew. Energy **119**, 809–819 (2018)
13. J.S. Kounsalye, P.B. Kharat, D.N. Bhoyar, K. Jadhav, Radiation-induced modifications in structural, electrical and dielectric properties of Ti 4 + ions substituted Li 0.5 Fe_2.5 O_4 nanoparticles. J. Mater. Sci. **29**, 8601–8609 (2018)
14. J.S. Kounsalye, P.B. Kharat, M.V. Shisode, K. Jadhav, Influence of Ti^{4+} ion substitution on structural, electrical and dielectric properties of Li0. 5Fe2. 5O4 nanoparticles. J. Mater. Sci. **28**, 17254–17261 (2017)
15. A.V. Humbe, P.B. Kharat, A.C. Nawle, K. Jadhav, Nanocrystalline Ni 0.70 – x Cu x Zn 0.30 Fe 2 O 4 with $0 \leq x \leq 0.25$ prepared by nitrate-citrate route: structure, morphology and electrical investigations. J. Mater. Sci. **29**, 3467–3481 (2018)
16. P.B. Kharat, J.S. Kounsalye, M.V. Shisode, K. Jadhav, Preparation and thermophysical investigations of $CoFe_2O_4$-based nanofluid: a potential heat transfer agent. J. Supercond. Novel Magn. (2018) https://doi.org/10.1007/s10948-018-4711-y
17. A. Bhattad, J. Sarkar, P. Ghosh, Improving the performance of refrigeration systems by using nanofluids: a comprehensive review. Renew. Sustain. Energy Rev. **82**, 3656–3669 (2018)
18. I. Mahbubul, E.B. Elcioglu, R. Saidur, M. Amalina, Optimization of ultrasonication period for better dispersion and stability of TiO2–water nanofluid. Ultrason. Sonochem. **37**, 360–367 (2017)
19. S. Umar, F. Sulaiman, N. Abdullah, S.N. Mohamad, Investigation of the effect of pH adjustment on the stability of nanofluid. In: AIP Conference Proceedings, AIP Publishing, pp. 020031 (2018)
20. M.N. Rashin, J. Hemalatha, Ultrasonics—An Effective Non-invasive Tool to Characterize Nanofluids, in Modeling, Methodologies, and Tools for Molecular and Nano-scale Communications. Springer, Berlin (2017), pp. 379–399
21. M. Leena, S. Srinivasan, Effects of rare earth doped on thermal conductivity of ZnO-water nanofluid by ultrasonic velocity measurements. Mater. Lett. **219**, 220–224 (2018)
22. B. Bellich, A. Gamini, J.W. Brady, A. Cesàro, Physico-chemical properties of aqueous drug solutions: from the basic thermodynamics to the advanced experimental and simulation results. Int. J. Pharm. **540**, 65–77 (2018)
23. M. Leena, S. Srinivasan, A comparative study on thermal conductivity of TiO2/ethylene glycol–water and TiO_2/propylene glycol–water nanofluids. J. Therm. Anal. Calorim. **131**, 1987–1998 (2018)
24. P.B. Kharat, A.R. Chavan, A.V. Humbe, K. Jadhav, Evaluation of thermoacoustics parameters of $CoFe_2O_4$–ethylene glycol nanofluid using ultrasonic velocity technique. J. Mater. Sci. (2018). https://doi.org/10.1007/s10854-018-0386-1
25. K. Anu, J. Hemalatha, Ultrasonic and magnetic investigations of the molecular interactions in zinc doped magnetite nanofluids. J. Mol. Liq. **256**, 213–223 (2018)
26. M.N. Rashin, J. Hemalatha, Magnetic and ultrasonic studies on stable cobalt ferrite magnetic nanofluid. Ultrasonics **54**, 834–840 (2014)
27. R. Paladhi, R. Singh, Miscibility and interaction studies on some aqueous polymer blend solutions by ultrasonic and rheological techniques. J. Appl. Polym. Sci. **51**, 1559–1565 (1994)
28. P.B. Kharat, A.V. Humbe, J.S. Kounsalye, K. Jadhav, Thermophysical investigations of ultrasonically assisted magnetic nanofluids for heat transfer, J. Supercond. Novel Magn. (2018) https://doi.org/10.1007/s10948-018-4819-0
29. S. Ayyappan, S. Mahadevan, P. Chandramohan, M. Srinivasan, J. Philip, B. Raj, Influence of Co^{2+} ion concentration on the size, magnetic properties, and purity of $CoFe_2O_4$ spinel ferrite nanoparticles. J. Phys. Chem. C **114**, 6334–6341 (2010)
30. T.H. Santos, J.P. Grilo, F.J. Loureiro, D.P. Fagg, F.C. Fonseca, D.A. Macedo, Structure, densification and electrical properties of Gd^{3+} and Cu^{2+} co-doped ceria solid electrolytes for SOFC applications: effects of Gd_2O_3 content. Ceram. Int. **44**, 2745–2751 (2018)
31. L. Kumar, P. Kumar, V. Kuncser, S. Greculeasa, B. Sahoo, M. Kar, Strain-induced magnetism and superexchange interaction in Cr substituted nanocrystalline cobalt ferrite. Mater. Chem. Phys. **211**, 54–64 (2018)
32. K. Srinivasamurthy, J. Angadi, S. Kubrin, S. Matteppanavar, D. Sarychev, P.M. Kumar, H.W. Azalea, B. Rudraswamy, Tuning of ferrimagnetic nature and hyperfine interaction of Ni^{2+} doped cobalt ferrite nanoparticles for power transformer applications. Ceram. Int. **44**, 9194–9203 (2018)
33. J. Mosayebi, M. Kiyasatfar, S. Laurent, Synthesis, functionalization, and design of magnetic nanoparticles for theranostic applications. Adv. Healthc. Mater. **6**, 1700306 (2017)

34. M.N. Rashin, J. Hemalatha, A novel ultrasonic approach to determine thermal conductivity in CuO–ethylene glycol nanofluids. J. Mol. Liq. **197**, 257–262 (2014)
35. M. Raja, R. Vijayan, P. Dineshkumar, M. Venkatesan, Review on nanofluids characterization, heat transfer characteristics and applications. Renew Sustain. Energy Rev. **64**, 163–173 (2016)
36. M.N. Rashin, J. Hemalatha, Magnetic and ultrasonic investigations on magnetite nanofluids. Ultrasonics **52**, 1024–1029 (2012)
37. A. Verdaguer, G. Sacha, H. Bluhm, M. Salmeron, Molecular structure of water at interfaces: wetting at the nanometer scale. Chem. Rev. **106**, 1478–1510 (2006)
38. P.A. Tomar, V.R. Shaikh, K.J. Patil, Tetraalkylammonium bromide-water mixtures revisited: isothermal compressibility and internal pressure variation in limiting concentration range at 298.15 K. J. Chem. Thermodyn. **126**, 119–125 (2018)
39. E. Abu-Nada, Dissipative particle dynamics investigation of heat transfer mechanisms in Al_2O_3-water nanofluid. Int. J. Therm. Sci. **123**, 58–72 (2018)
40. A. Riaud, M. Baudoin, O.B. Matar, J.-L. Thomas, P. Brunet, On the influence of viscosity and caustics on acoustic streaming in sessile droplets: an experimental and a numerical study with a cost-effective method. J. Fluid Mech. **821**, 384–420 (2017)
41. M. Sheikholeslami, Numerical investigation for CuO-H2O nanofluid flow in a porous channel with a magnetic field using the mesoscopic method. J. Mol. Liq. **249**, 739–746 (2018)
42. Y. Ma, R. Mohebbi, M.M. Rashidi, O. Manca, Z. Yang, Numerical investigation of MHD effects on nanofluid heat transfer in a baffled U-shaped enclosure using lattice Boltzmann method. J. Therm. Anal. Calorim. (2018). https://doi.org/10.1007/s10973-018-7518-y
43. L. Xiao, J. Li, D.F. Brougham, E.K. Fox, N. Feliu, A. Bushmelev, A. Schmidt, N. Mertens, F. Kiessling, M. Valldor, Water-soluble superparamagnetic magnetite nanoparticles with biocompatible coating for enhanced magnetic resonance imaging. ACS Nano **5**, 6315–6324 (2011)